Electronic Supplementary Information

High-efficiency photodriven coupling of CO_2 and various epoxides via multi-shelled hollow ZIF/MXene derived composite with low activation energy

Yang Wang,[a] Meili Ding,[a,b,*] Xiaotong Fu[a] and Jianfeng Yao[a,*]

[a]College of Chemical Engineering, Jiangsu Co-Innovation Center of Efficient Processing and Utilization of Forest Resources, Nanjing Forestry University, Nanjing, Jiangsu 210037, China.
[b]FRAPP'S Chemical Industry Co., Ltd, Lishui, Zhejiang 323316, China.
*Corresponding author.
Email: mlding@njfu.edu.cn; jfyao@njfu.edu.cn

S1. Experimental details

Materials

All chemicals in this study are obtained commercially and directly used without further purification. Cobaltous nitrate hexahydrate ($Co(NO_3)_2 \cdot 6H_2O$, analytical reagent (AR)), ascorbic acid (AA, AR), and methanol (AR) were obtained from Sinopharm Chemical Reagent Co., Ltd. Zinc nitrate hexahydrate ($Zn(NO_3)_2 \cdot 6H_2O$, 99%), hydrochloric acid (HCl, AR), and silver nitrate (AR) were purchased from Nanjing Chemical Reagent Co., Ltd. Cyclohexene oxide (98%), epoxypropyl phenyl ether (99%), and 1,2-epoxy butane (99%) were obtained from energy chemical. ECH (99.5%), bromopropylene oxide (98%), 1,2-epoxyhexane (99%), benzylmethoxymethyloxirane (99%), 2-methylimidazole (98%), ethyl acetate (AR), tetramethylammonium hydroxide (TMAOH, 10 wt% in water), and tetrabutyl ammonium bromide (TBAB, 99%) were provided from Aladdin industrial Co., Ltd. Lithium fluoride (LiF, AR), ammonium hydroxide ($NH_3 \cdot OH$, 25-28%) and polyvinyl pyrrolidone with an average molar mass of 24,000 g/mol were obtained from Shanghai Macklin Biochemical Technology Co., Ltd. Aluminium titanium carbide (Ti_3AlC_2,

98%) was purchased from Rhön Reagent.

Synthesis of 4L-ZIF

Typically, 0.86 g $Zn(NO_3)_2 \cdot 6H_2O$ and 0.98 g 2-methylimidazole were dissolved in 30 mL and 5 mL methanol, respectively, by ultrasound and stirred for 5 min at room temperature (RT). After that, the solution of zinc salt was poured into the solution of 2-methylimidazole solution quickly. The mixture was stirred for 1 min and then kept undisturbed for 24 h. After washing with methanol three times and drying at 80 °C under vacuum for 12 h, ZIF-8 crystals were obtained. 90 mg ZIF-8 powder was dispersed in 30 mL methanol by ultrasonication for 20 min to give a suspension solution with a concentration of 3 mg/mL. 150 mg $Co(NO_3)_2 \cdot 6H_2O$ and 10 mL methanol solution of 2-methylimidazole were added successively in the above suspension solution of ZIF-8. After 24 h stirring (500 rpm) at RT, ZIF-8@ZIF-67 (2L-ZIF) was obtained by washing with methanol three times and drying at 80 °C under vacuum for 12 h. After repeating the same procedures, a quadruple-layer structure 4L-ZIF was prepared.

Synthesis of MXene sheets

Typically, LiF (1 g, 0.039 mol) and Ti_3AlC_2 (1 g, 0.005 mol) were slowly added to a polytetrafluoroethylene beaker containing 20 mL HCl (9 mol/L), and then kept stirred (550 rpm) at 50 °C for 72 h. After etching, the resultant mixture was cooled to RT naturally and washed with deionized water several times until pH reached 7. The multiple-layer MXene powder was collected by freeze-drying for at least 12 h. A facile hydrothermal-assisted intercalation strategy was employed to give MXene sheets. Specifically, 0.1 g multilple-layer MXene powder was dispersed in 30 mL TMAOH aqueous solution (10 wt%). 0.176 g AA was then added and the mixture was stirred for 10 min. The mixture was transferred into a 200 mL round-bottom flask and heated at 140 °C for 24 h. Black precipitate was obtained by washing with deionized water until neutral pH. Subsequently, the black precipitate was dispersed in methanol and sonicated in an ice bath and under nitrogen atmosphere for 1 h. Finally, MXene sheets were collected by centrifugation at 3500 rpm for 30 min.

Characterization

The X-ray diffraction (XRD) analysis of the samples was conducted using a Rigaku Ultima IV instrument. The Fourier Transform Infrared (FT-IR) spectra were recorded with a Thermo Electron Nicolet-360 spectrometer. The morphology of catalysts was examined through scanning electron microscopy (SEM) using a Regulus 8100 microscope, operating at an acceleration voltage of 15 kV. Transmission electron microscopy (TEM) images were captured using JEOL JEM-2100 equipment. X-ray photoelectron spectroscopy (XPS) analyses were performed on an AXIS Ultra DLD XPS spectrometer, utilizing Al Ka as the excitation source. The adsorption-desorption isotherms for CO_2 and N_2 were measured using a TriStar 3020 micrometric fully automated volumetric adsorption apparatus. UV-visible diffuse reflectance spectra were acquired with a Shimadzu UV-2600 spectrophotometer. Electrochemical measurements were carried out on a CHI-760E electrochemical workstation. Steady-state photoluminescence (PL) data were obtained using an Edinburgh FLS1000 instrument. Catalytic yield and selectivity were determined with a gas chromatography (HF-901A, Shandong Huifen Instrument Co., Ltd., China), equipped with a flame ionization detector and utilizing high-purity N_2 as the carrier gas.

Table S1. The catalytic CO_2 cycloaddition of ECH over 4L-ZIF/MX-X (X = 2, 4, 6, 8, 10, 15, 20 or 40) with different initial mass ratio of 4L-ZIF and MXene sheets.[a]

Catalyst	Selectivity (%)	Yield[b] (%)
4L-ZIF/MX-2	>99	67
4L-ZIF/MX-4	>99	70
4L-ZIF/MX-6	>99	72
4L-ZIF/MX-8	>99	75
4L-ZIF/MX-10	>99	73
4L-ZIF/MX-15	>99	69
4L-ZIF/MX-20	>99	65
4L-ZIF/MX-40	>99	57

[a] Reaction condition: catalyst (50 mg), TBAB (0.2 mmol), ECH (5 mmol), 1 bar CO_2, Xe lamp irradiation (350 mW/cm^2), 6 h. [b] Determined by GC.

Table S2 Comparison of CoNHPC/TM-8 with other reported hollow-structured MOF based catalysts for the photodriven CO_2 cycloaddition with ECH.

Entry	Catalysts	Reaction conditions	Yield (%)	References
1	CoNHPC/TM-8	0.1 MPa, 350 mW/cm^2, 6 h	96%	This work
2	HPC-800	0.1 MPa, 300 mW/cm^2, 10 h	94%	S1
3	MOF-74-HT	0.1 MPa, 150 mW/cm^2, 18 h	89%	S2
4	CuS@HKUST-1	0.1 MPa, 300 mW/cm^2, 18 h	88%	S3
5	BHNC-900	0.1 MPa, 300 mW/cm^2, 8 h	94%	S4
6	ZNC-800	0.1 MPa, 1000 mW/cm^2, 12 h	91%	S5
7	Zn SA-NC	0.1 MPa, 300 mW/cm^2, 16 h	97%	S6

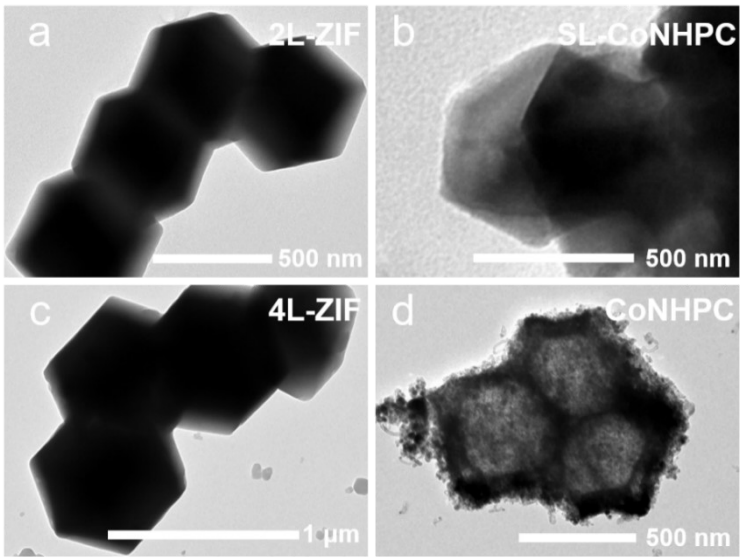

Fig. S1 TEM images of (a) ZIF-8@ZIF-67 (2L-ZIF), (b) 2L-ZIF derived SL-CoNHPC, (c) 4L-ZIF, and (d) CoNHPC.

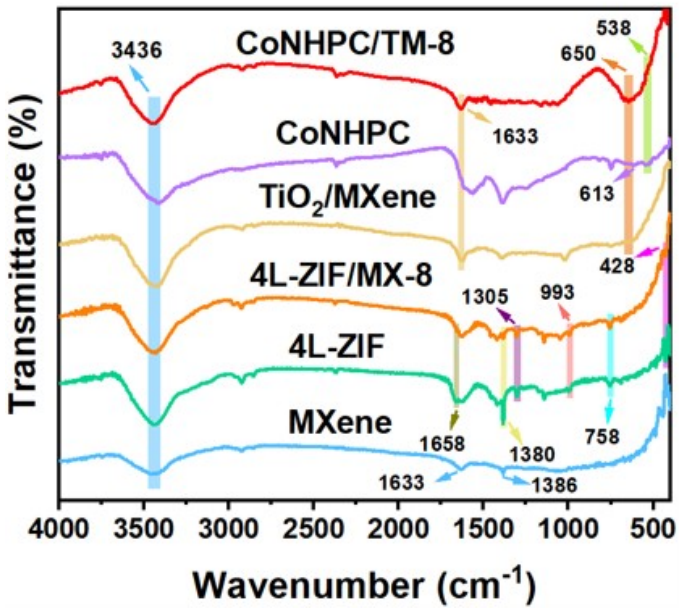

Fig. S2 FT-IR spectra of CoNHPC/TM-8, CoNHPC, TiO_2/MXene, 4L-ZIF/MX-8, 4L-ZIF, and MXene sheets.

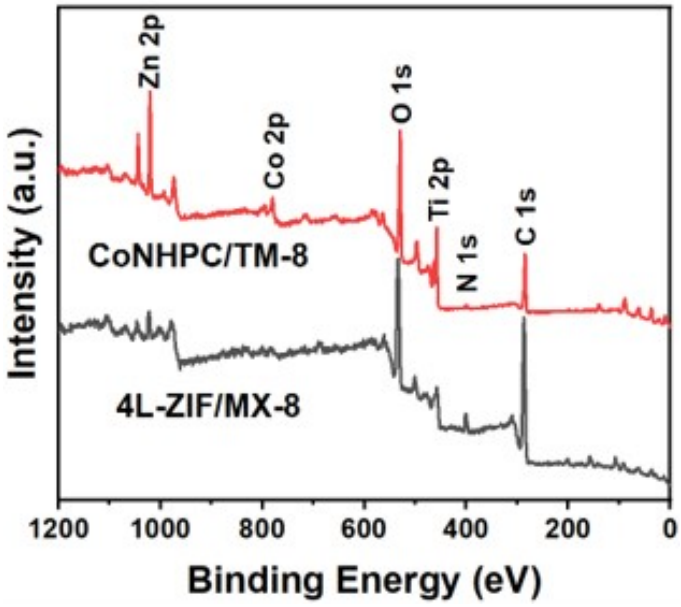

Fig. S3 XPS survey scans for 4L-ZIF/MX-8 and CoNHPC/TM-8.

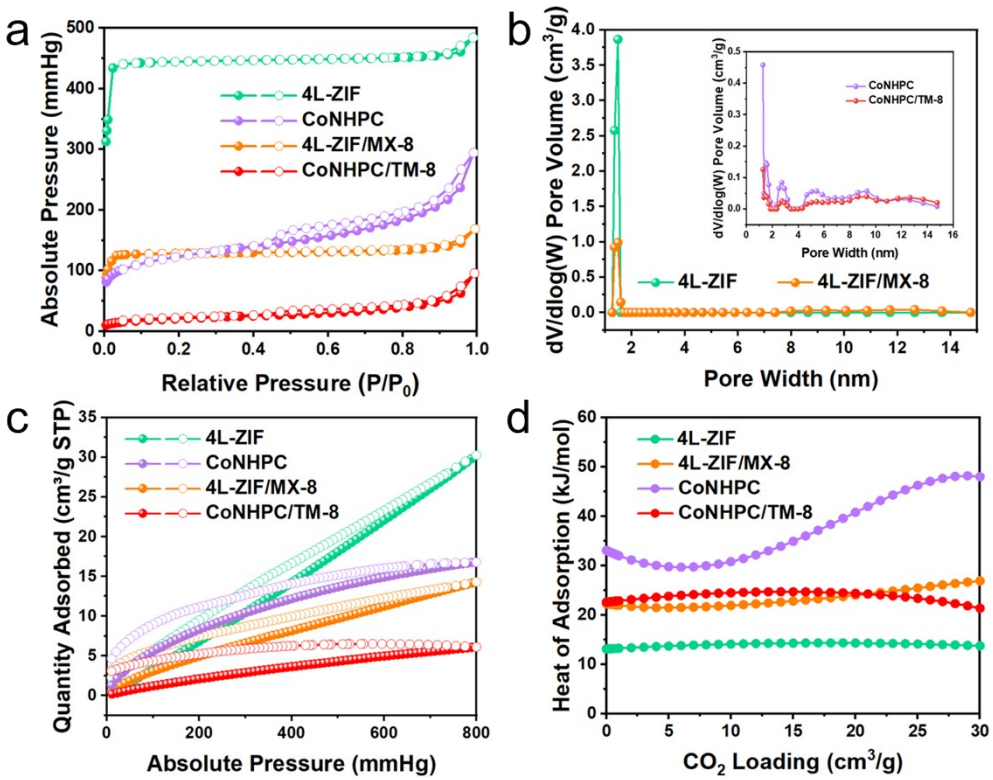

Fig. S4 (a) N_2 adsorption–desorption isotherms at 77 K, (b) pore size distribution curve, (c) CO_2 adsorption–desorption isotherm at 273 K, and (d) isovolumic heat of adsorption of CO_2 for CoNHPC/TM-8, CoNHPC, 4L-ZIF/MX-8 and 4L-ZIF.

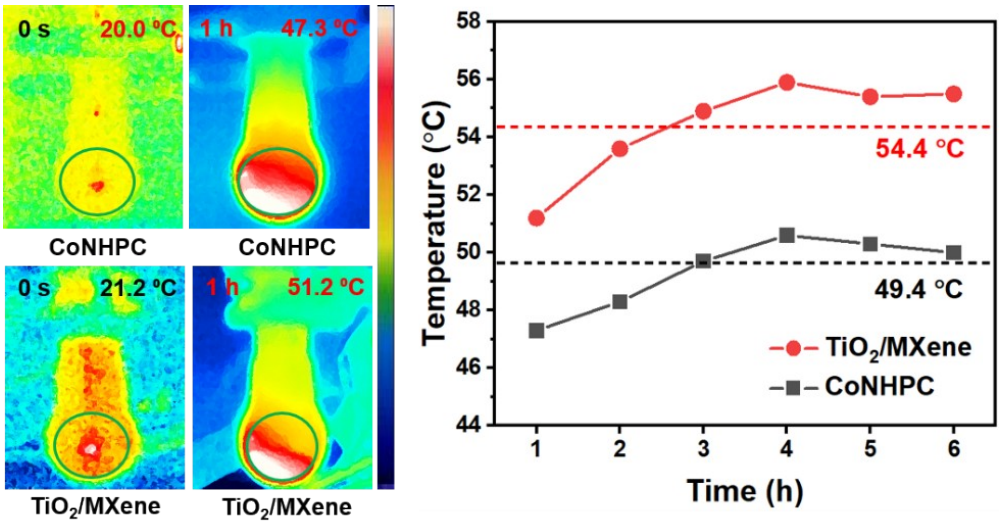

Fig. S5 Infrared thermogram images and center temperature of CoNHPC and TiO_2/MXene over time upon light irradiation.

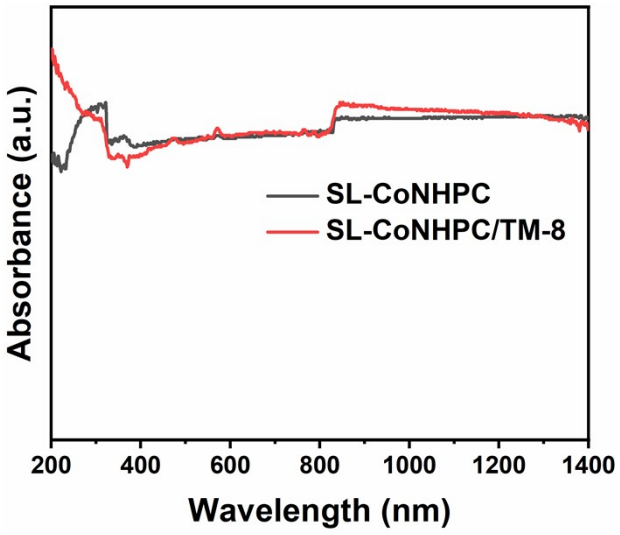

Fig. S6 UV–Vis DRS spectra of 2-ZIF derived SL-CoNHPC and SL-CoNHPC/TM-8.

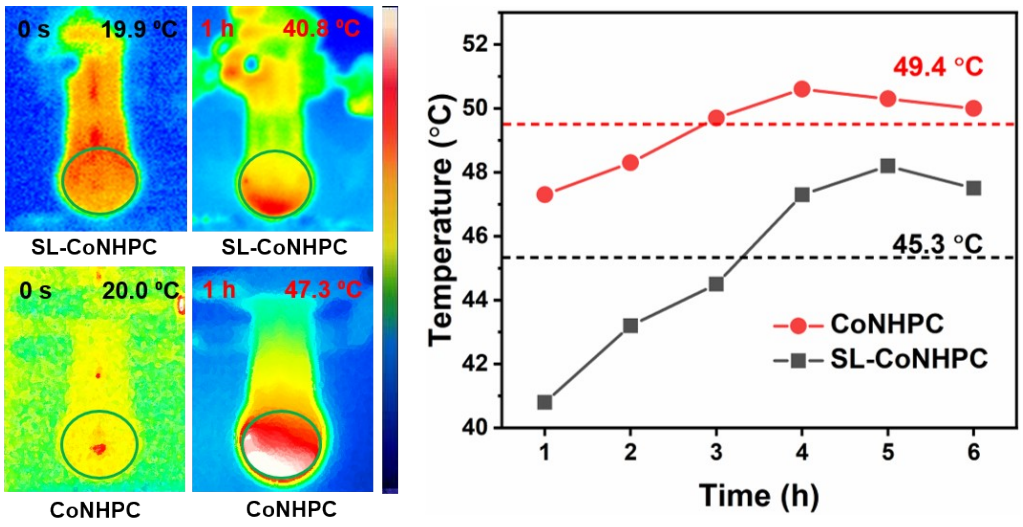

Fig. S7 Infrared thermogram images and center temperature of SL-CoNHPC and CoNHPC over time upon light irradiation.

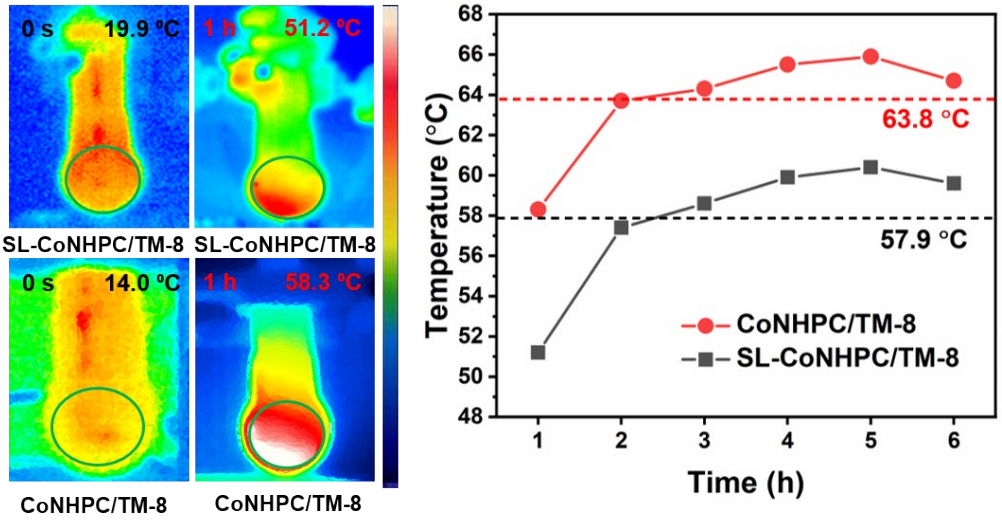

Fig. S8 Infrared thermogram images and center temperature of SL-CoNHPC/TM-8 and CoNHPC/TM-8 over time upon light irradiation.

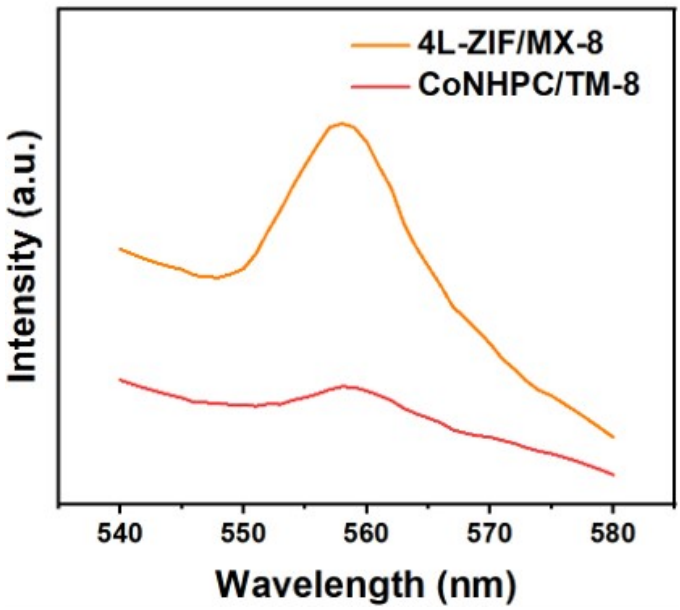

Fig. S9 PL spectra of CoNHPC/TM-8 and 4L-ZIF/MX-8.

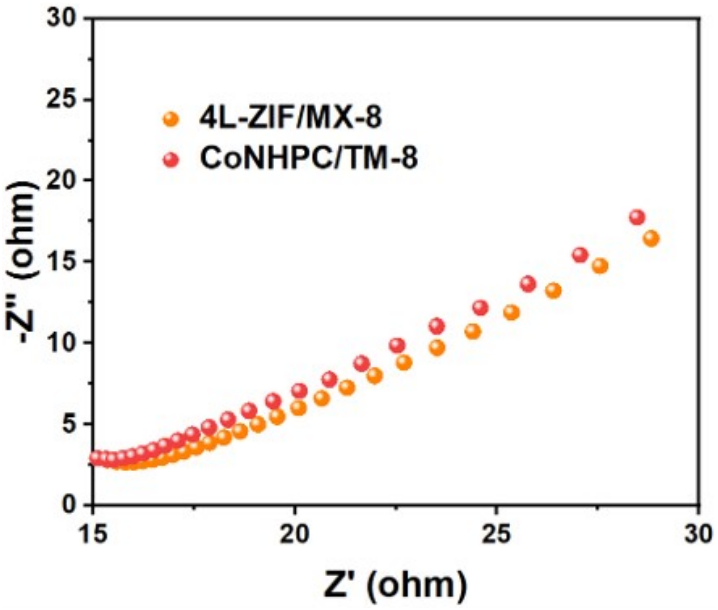

Fig. S10 EIS of CoNHPC/TM-8 and 4L-ZIF/MX-8.

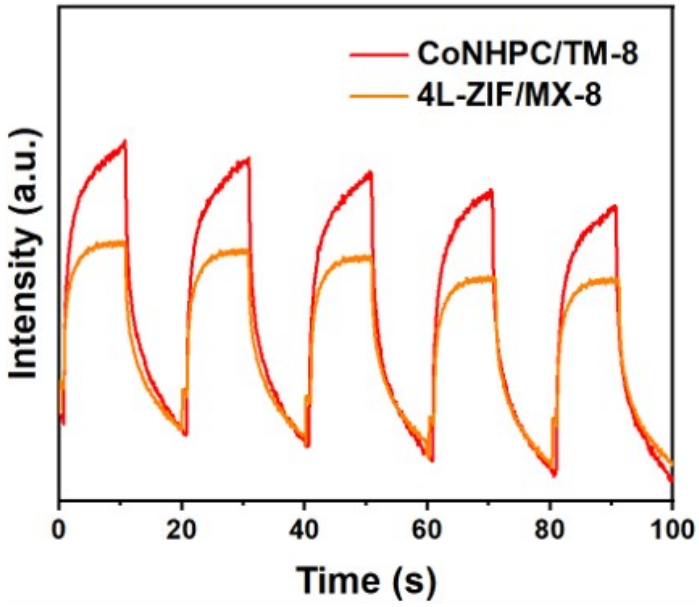

Fig. S11 Transient photocurrent responses of CoNHPC/TM-8 and 4L-ZIF/MX-8.

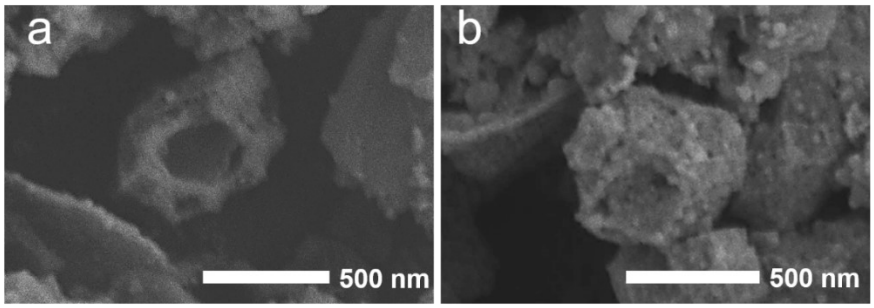

Fig. S12 SEM images of (a) CoNHPC/TM-8 and (b) solid CoNHPC/TM-8.

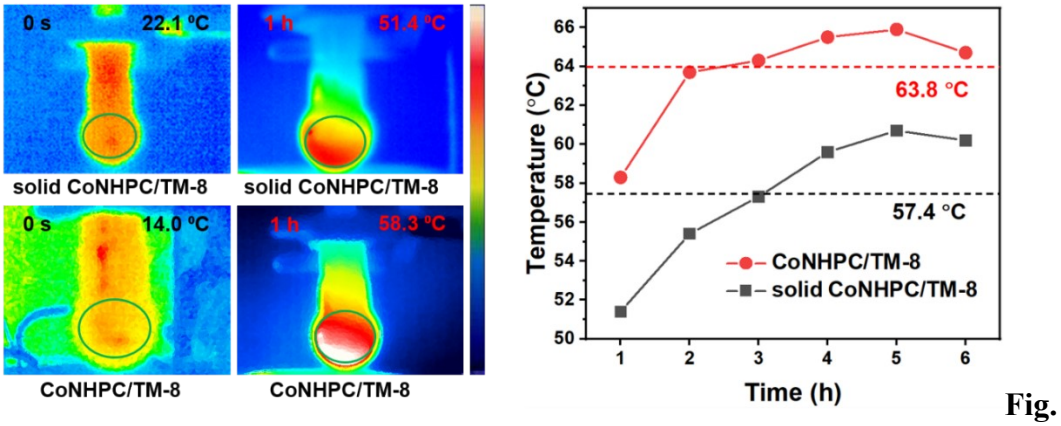

Fig. S13 Infrared thermogram images and center temperature of CoNHPC/TM-8 and solid CoNHPC/TM-8 over time upon light irradiation.

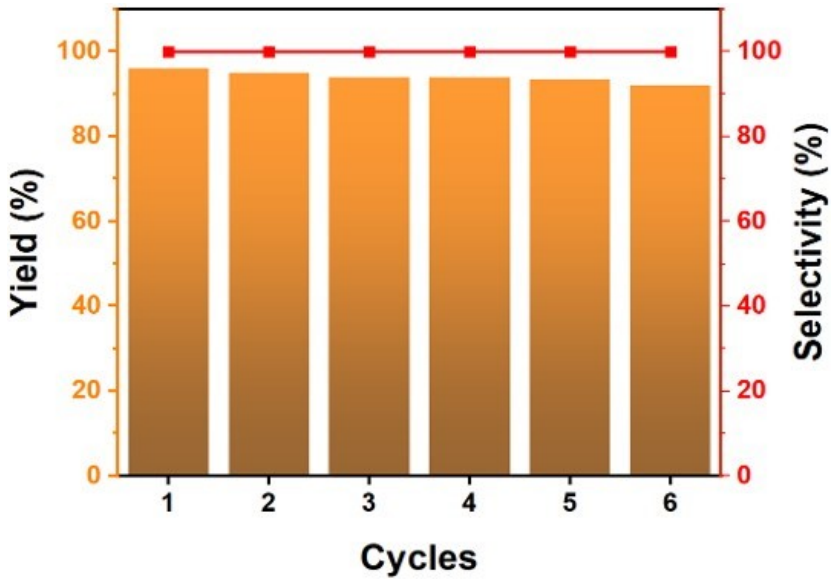

Fig. S14 Recycling tests of CoNHPC/TM-8 for the cycloaddition of CO_2 with ECH.

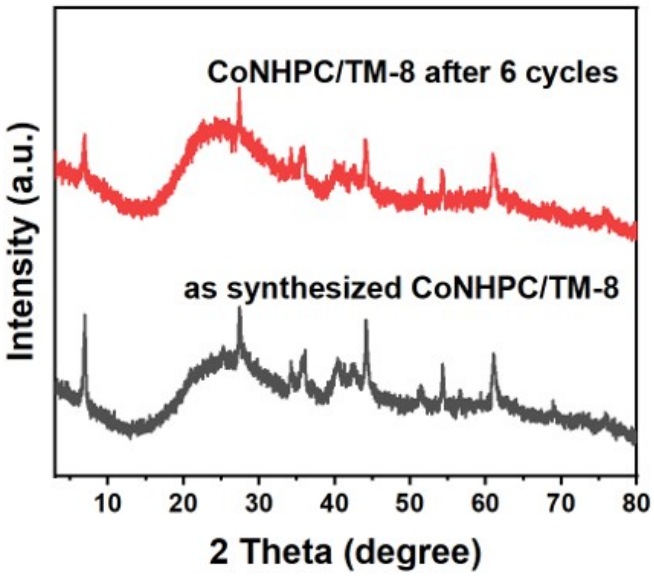

Fig. S15 Powder XRD patterns of CoNHPC/TM-8 before and after 6 cycles of catalytic CO_2 cycloaddition.

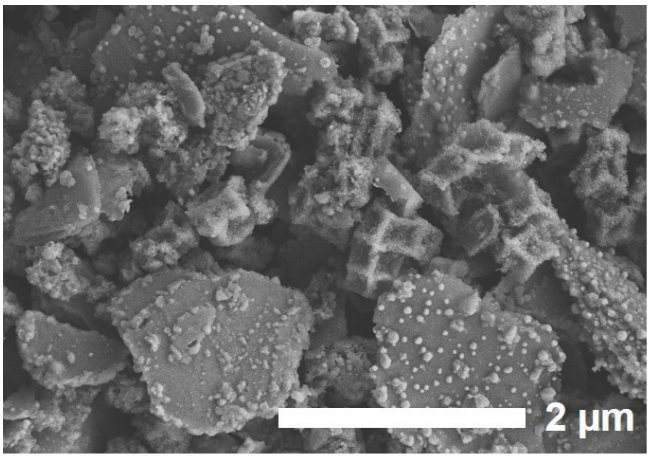

Fig. S16 SEM image of CoNHPC/TM-8 after 6 cycles of catalytic CO_2 cycloaddition.

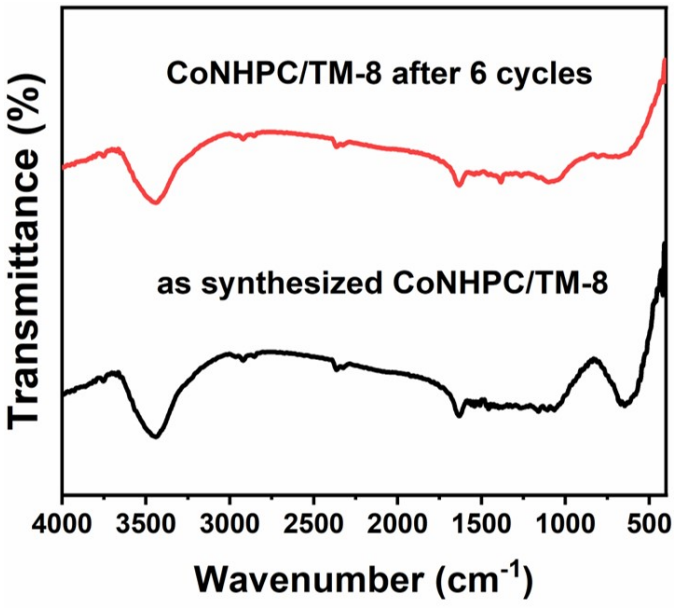

Fig. S17 FT-IR spectra of CoNHPC/TM-8 before and after 6 cycles of catalytic CO_2 cycloaddition.

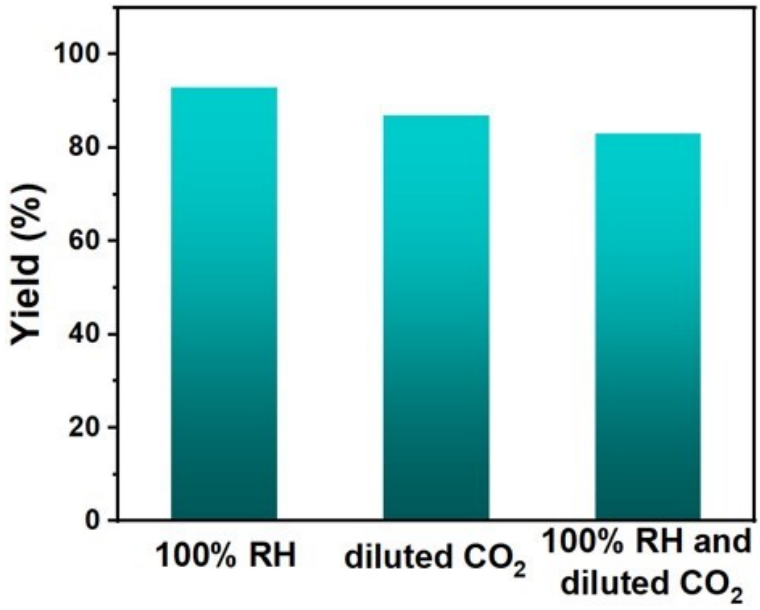

Fig. S18 Catalytic performance of the CoNHPC/TM-8 catalyst under different conditions.

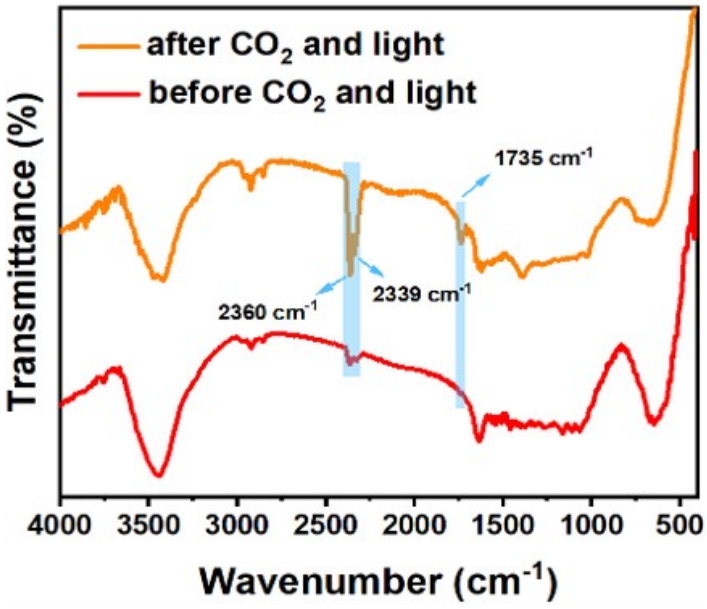

Fig. S19 FT-IR spectra of CoNHPC/TM-8 under CO_2 atmosphere and light irradiation.

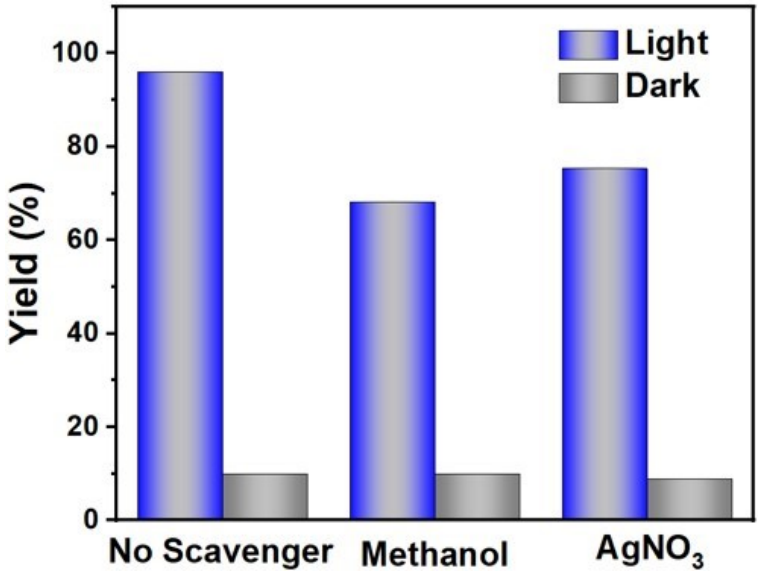

Fig. S20 Effect of different scavengers on CO_2 cycloaddition catalyzed by CoNHPC/TM-8.

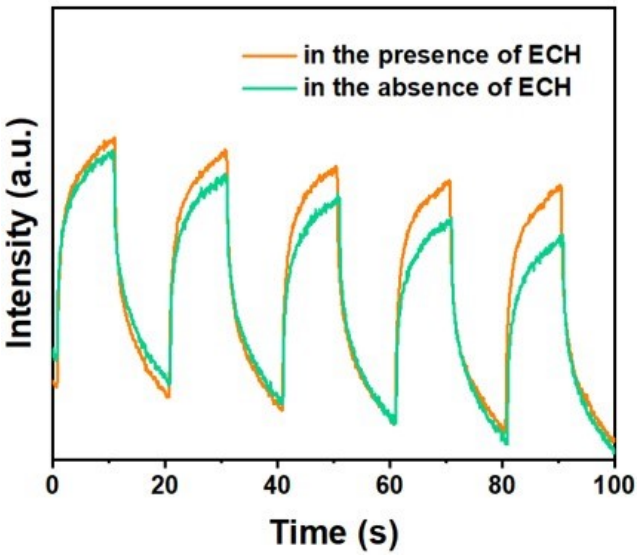

Fig. S21 The photo-current density of CoNHPC/TM-8 in the presence and absence of ECH.

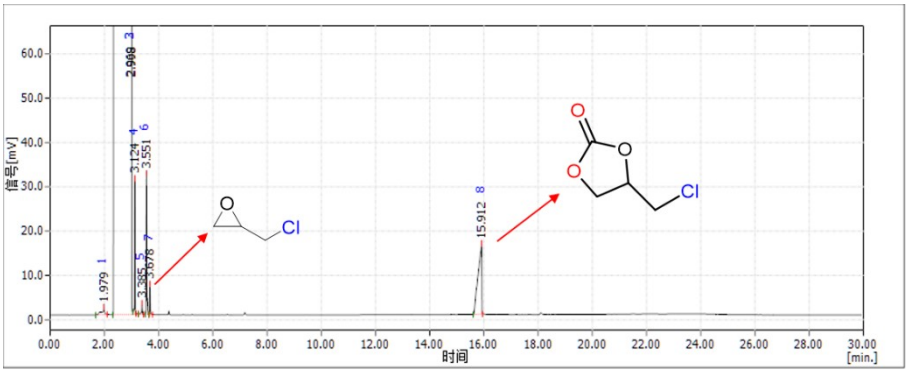

Fig. S22 Gas chromatogram of CO_2 cycloaddition with ECH catalyzed by CoNHPC/TM-8.

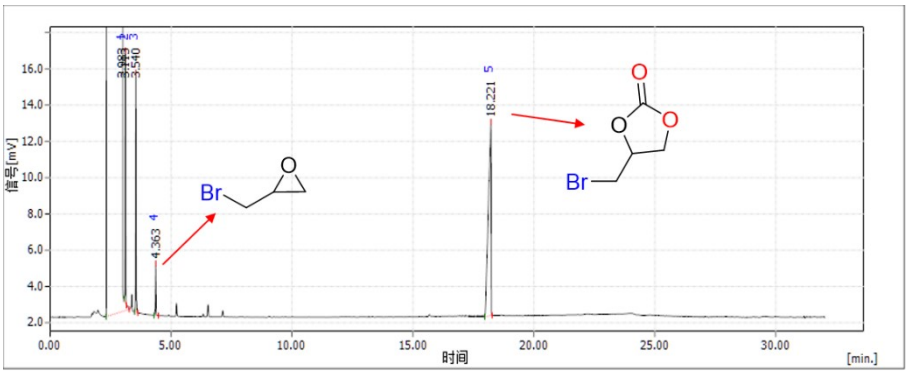

Fig. S23 Gas chromatogram of CO_2 cycloaddition with bromopropylene oxide catalyzed by CoNHPC/TM-8.

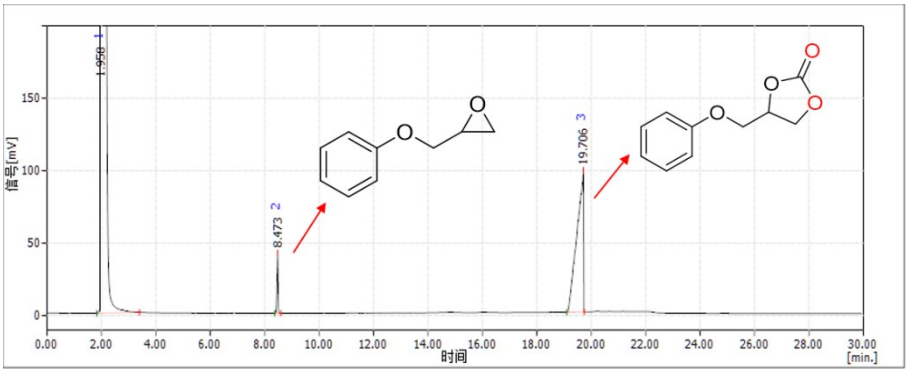

Fig. S24 Gas chromatogram of CO_2 cycloaddition with styrene oxide catalyzed by CoNHPC/TM-8.

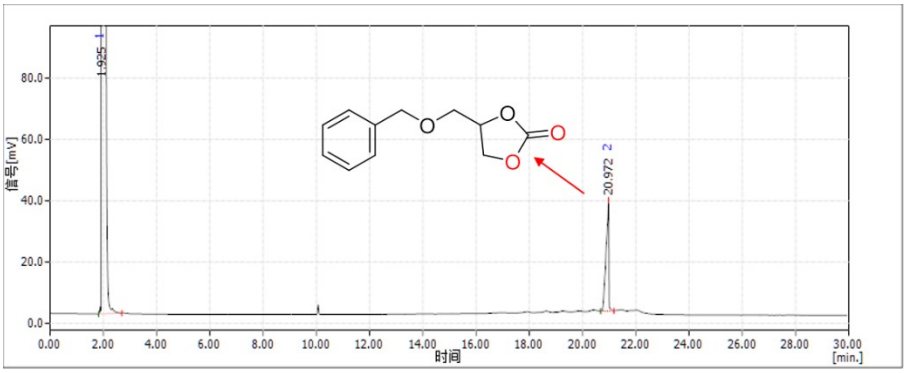

Fig. S25 Gas chromatogram of CO_2 cycloaddition with benzylmethoxymethyloxirane catalyzed by CoNHPC/TM-8.

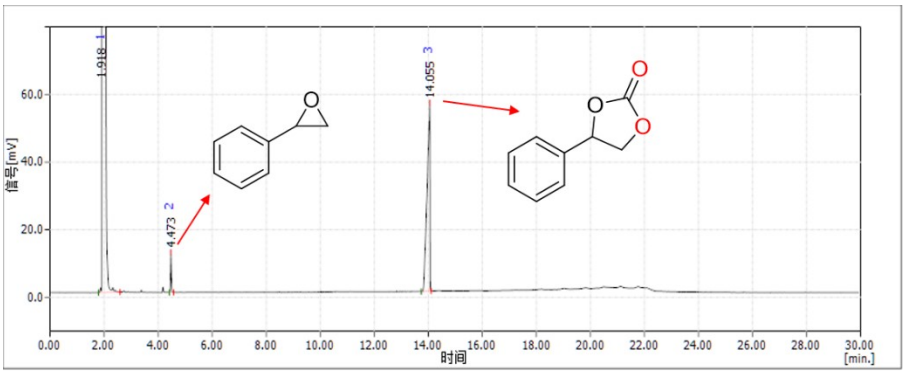

Fig. S26 Gas chromatogram of CO_2 cycloaddition with epoxypropyl phenyl ether catalyzed by CoNHPC/TM-8.

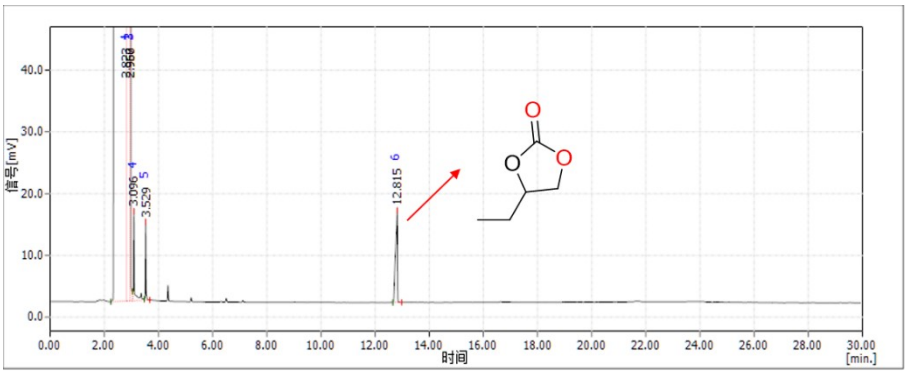

Fig. S27 Gas chromatogram of CO_2 cycloaddition with 1,2-epoxy butane catalyzed by CoNHPC/TM-8.

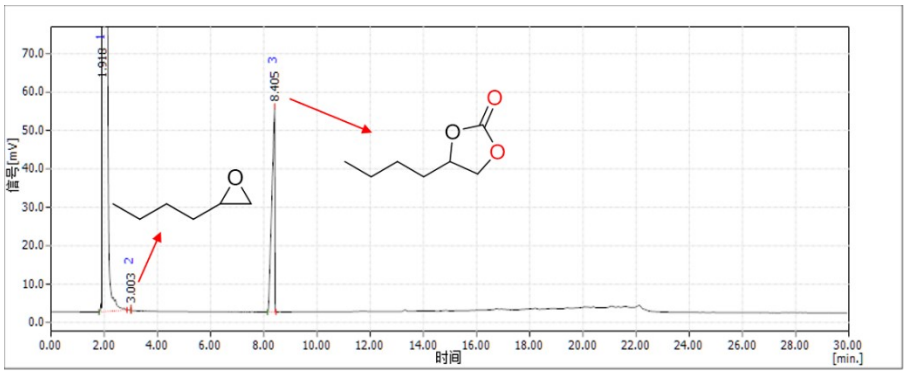

Fig. S28 Gas chromatogram of CO_2 cycloaddition with 1,2-epoxyhexane catalyzed by CoNHPC/TM-8.

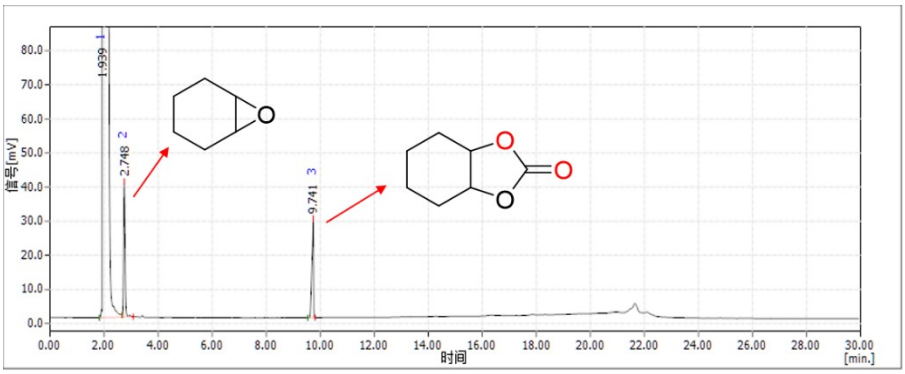

Fig. S29 Gas chromatogram of CO_2 cycloaddition with cyclohexene oxide catalyzed by CoNHPC/TM-8.

References

S1 Q. Yang, C.-C. Yang, C.-H. Lin and H.-L. Jiang, Metal–organic-framework-derived hollow N-doped porous carbon with ultrahigh concentrations of single Zn atoms for efficient carbon dioxide conversion, *Angew. Chem., Int. Ed.*, 2019, **58**, 3511-3515.

S2 H. Chen, L. Shao, C. Wang and Y. Fu, Construction of a hierarchical tubular metal–organic framework composed of nanosheet arrays as a photothermal catalyst through phase transformation, *J. Mater. Chem. A*, 2022, **10**, 17434-17439.

S3 H. Zhu, Q. Shen, Y. Yuan, H. Gao, S. Zhou, F.-L. Yang, L. Sun, X. Wang, J. Yi and X. Han, Engineering the sulfide semiconductor/photoinactive-MOF heterostructure with a hollow cuboctahedral structure to enhance photocatalytic CO_2-epoxide-cycloaddition efficiency, *Inorg. Chem.*, 2024, **63**, 4078-4085.

S4 T. Wang, F. Chen, H. An, K. Chen and J. Gao, Metal-organic-framework-derived boron and nitrogen dual-doped hollow mesoporous carbon for photo-thermal catalytic conversion of CO_2, *J. Solid State Chem.*, 2024, **332**, 124570.

S5 Y. Liu, Y. Chen, Y. Liu, Z. Chen, H. Yang, Z. Yue, Q. Fang, Y. Zhi and S. Shan, Zn and N co-doped porous carbon nanosheets for photothermally-driven CO_2 cycloaddition, *J. Catal.*, 2022, **407**, 65-76.

S6 D. Liu, S. Kang, Y. Xu, P. Duan and S. Chen, Core-shell catalyst with synergistic hydroxyl and nitrogen active sites for CO_2 cycloaddition, *J. Environ.*, 2021, **9**, 106452.